Int. J. Multiphase Flow Vol. 19, No. 1, pp. 213–228, 1993
Printed in Great Britain.

0301-9322/93 $6.00 + 0.00

MASS TRANSFER AROUND A MOVING ENCAPSULATED LIQUID DROP

H. HASHIMOTO and S. KAWANO
Institute of Fluid Science, Tohoku University, 2-1-1 Katahira, Aobaku, Sendai 980, Japan

(Received 13 June 1991; in revised form 1 September 1992)

Abstract—The characteristics of forced-convection mass transfer around a moving gas–liquid compound encapsulated drop, assumed to be spherical and concentric, are studied numerically under the condition of uniform concentration at the outer interface. Numerical solutions of the Navier–Stokes equations and the diffusion equation including the first-order chemical reaction term have been obtained up to Re = 200. The effects of the inner and outer radii of the encapsulated drop, the physical properties of the fluids and the chemical reaction rate on the mass transfer coefficient are investigated quantitatively. The dependence of the concentration contours on the streamlines around the encapsulated drop is discussed in detail. Results of numerical predictions of the mass transfer coefficient are compared with previous results of the same for a gas bubble, for a liquid drop and for a rigid sphere. The work suggests the possibility of highly functional mass exchange by applying encapsulated drops as spherical liquid membranes.

Key Words: gas–liquid compound drop, encapsulated liquid drop, mass transfer, chemical reaction, numerical analysis, bubble, liquid drop, rigid sphere

INTRODUCTION

The gas–liquid compound encapsulated drop, i.e. a spherical gas bubble coated with a thin liquid film, has received considerable attention because it has highly functional applications. For example, the encapsulated drop could be applied to spherical liquid membranes with selectivity (Li 1971), direct-contact heat and mass exchangers and artificial blood oxygenations (e.g. Johnson & Sadhal 1985). Furthermore, the spherical solid shell produced by solidifying the encapsulated drop could be applied to high-performance solid fuels, artificial organs, lightweight structural materials, buoyant catalytic agents, energy storage systems and so on (Lee *et al.* 1986). Johnson & Sadhal (1985) reviewed the previous research on compound multiphase drops and revealed that rigorous fluid-mechanical analysis was essential for such applications of gas–liquid compound encapsulated drops.

Recently, more fluid-dynamical analyses of encapsulated drops have been reported. The formation mechanism of the encapsulated drop was studied by Mori (1987), Greene *et al.* (1988), Hashimoto & Kawano (1989, 1990) and Kawano & Hashimoto (1990) using liquid–liquid–gas systems, and by Kendall (1986) and Lee & Wang (1986) using annular nozzles. The oscillating motion of the encapsulated drop interfaces was studied by Landman (1985), Tsamopoulos & Brown (1987), Lee & Wang (1988) and Stone & Leal (1990). Furthermore, various sequential production devices of relatively large spherical solid shells (up to 8 mm dia) using thermofluid dynamical effects were designed by Lee *et al.* (1986) and Hashimoto & Kawano (1991). Consequently, the mass production technique of stable encapsulated drops is considered to have reached the stage of practical use.

For the applications described above, it is necessary to investigate the heat and mass transfer characteristics around an encapsulated drop moving at finite velocity. There are some reports relating to the forced-convection heat and mass transfer around an encapsulated drop (Rushton & Davies 1983; Sadhal & Oguz 1985; Oguz & Sadhal 1987; Vuong & Sadhal 1989a, b). However, they are useful only in a creeping flow, i.e. they are based on Stokes' approximation theory. No data on basic theoretical research on the inertia effect of the flow around an encapsulated drop are available.

In the present paper, the characteristics of mass transfer around a moving encapsulated drop, assumed to be spherical and concentric, were studied numerically up to Reynolds numbers (Re) of 200 while the material underwent a first-order chemical reaction in the continuous phase.

Mass transfer coefficients were obtained from the numerical solutions of the Navier–Stokes equations and the diffusion equation under certain boundary conditions for the wide velocity range and for varying physical properties of the fluids. The dependence of the concentration contours on the streamlines is discussed based on computational visualizations. This report provides a basic understanding of the phenomena and the development of a highly functional mass exchanger using spherical liquid membranes with selectivity.

THEORETICAL DEVELOPMENT

Mathematical Model

A spherical encapsulated liquid (phase 1) drop, radius ζ' moving at a constant velocity U_∞ through another immiscible fluid (phase 2), was the subject of research. The following assumptions are used in the analysis based on experimental data (e.g. Hashimoto & Kawano 1990):

(1) The fluids are Newtonian and the flow is steady, viscous, incompressible and axisymmetric.
(2) The physical properties are constant; therefore, the flow analysis is decoupled from the diffusion equation.
(3) The effects of gravity force and the inner gas motion are negligibly small.
(4) The encapsulated drop consists of a spherical gas bubble coated with a concentric liquid film.
(5) The oscillations of encapsulated drop interfaces are neglected.
(6) The encapsulated drop always has a uniform constant concentration C_I, where C is concentration and the subscript I indicates the value at the encapsulated drop outer interface.
(7) Only the first-order chemical reaction is considered, i.e. the original material A changes into material B with reaction rate K in a moment. The diffusion of material B is neglected.

In our previous paper (Kawano & Hashimoto 1992) it was reported that some encapsulated drops were nearly spherical for $\mathrm{Re} \leqslant 300$, and that the inner and outer interfaces of the encapsulated drop with a thin liquid film and under large interface tensions were nearly concentric. Here, $\mathrm{Re} = 2\zeta' \rho_2 U_\infty / \eta_2$ represents the encapsulated drop Reynolds number, η is the fluid viscosity,

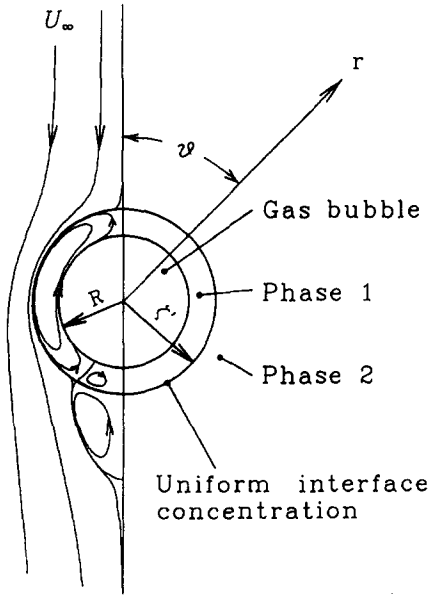

Figure 1. Schematic of the coordinate system and typical streamlines (at Re = 100, $\zeta = 1.4$, $\kappa = 0.959$ and $\gamma = 1.21$) for an encapsulated liquid drop.

ρ is the fluid density and the subscript 2 indicates phase 2. The state of assumption (6) seems to actually stand when $C_1 \gg C_\infty$ is satisfied, whereby the subscript ∞ indicates the value at a large distance from the outer interface of the encapsulated drop. Although numerical study for the deformation of the encapsulated drop interfaces will become necessary, the purpose of this paper is to explore applications of the encapsulated drop as the first step. The schematic of the theoretical model, typical streamlines and the coordinate system are shown in figure 1.

Basic Equations

The Navier–Stokes equations for steady, viscous, incompressible and axisymmetric flow in terms of the stream function ψ and vorticity ω are written in spherical coordinates (r, ϑ) as follows:

$$E^2\psi_i = \omega_i r \cdot \sin\vartheta \tag{1}$$

and

$$\frac{\hat{\mathrm{Re}}_i}{2}\left[\frac{\partial\psi_i}{\partial r}\cdot\frac{\partial}{\partial\vartheta}\left(\frac{\omega_i}{r\cdot\sin\vartheta}\right)-\frac{\partial\psi_i}{\partial\vartheta}\cdot\frac{\partial}{\partial r}\left(\frac{\omega_i}{r\cdot\sin\vartheta}\right)\right]\sin\vartheta = E^2(\omega_i r\cdot\sin\vartheta), \tag{2}$$

where

$$E^2 = \frac{\partial^2}{\partial r^2}+\frac{\sin\vartheta}{r^2}\cdot\frac{\partial}{\partial\vartheta}\left(\frac{1}{\sin\vartheta}\cdot\frac{\partial}{\partial\vartheta}\right), \tag{3}$$

$\hat{\mathrm{Re}}_i = 2R\rho_i U_\infty/\eta_i$ is the gas bubble Reynolds number, R is the inner gas bubble radius and the subscript i is equal to 1 or 2 and indicates phase 1 or 2, respectively. Continuity equations are automatically satisfied by introducing ψ. The velocity components V are related to ψ by

$$V_{r,i} = \frac{-1}{r^2\cdot\sin\vartheta}\cdot\frac{\partial\psi_i}{\partial\vartheta}, \quad V_{\vartheta,i} = \frac{1}{r\cdot\sin\vartheta}\cdot\frac{\partial\psi_i}{\partial r}, \tag{4}$$

where subscripts r and ϑ indicate the radial and tangential direction, respectively.

The appropriate dimensionless diffusion equation for phase 2 with a first-order chemical reaction in the spherical coordinates is as follows:

$$\frac{\partial C}{\partial t}+V_{r,2}\frac{\partial C}{\partial r}+\frac{V_{\vartheta,2}}{r}\cdot\frac{\partial C}{\partial\vartheta} = \frac{2\zeta}{\mathrm{Re}\cdot\mathrm{Sc}}\cdot\left[\frac{1}{r^2}\cdot\frac{\partial}{\partial r}\left(r^2\frac{\partial C}{\partial r}\right)+\frac{1}{r^2\cdot\sin\vartheta}\cdot\frac{\partial}{\partial\vartheta}\left(\sin\vartheta\frac{\partial C}{\partial\vartheta}\right)-K\cdot C\right], \tag{5}$$

where $\mathrm{Sc} = \eta_2/(D\rho_2)$ is the Schmidt number, D is the diffusivity of material A in phase 2 and t is time.

All quantities have been made dimensionless using the following forms:

$$r = \frac{r'}{R}, \quad \zeta = \frac{\zeta'}{R}, \quad \psi_i = \frac{\psi_i'}{U_\infty R^2}, \quad \omega_i = \frac{\omega_i' R}{U_\infty},$$
$$V = \frac{V'}{U_\infty}, \quad K = \frac{R^2K'}{D}, \quad C = \frac{C'-C_\infty}{C_1-C_\infty}, \quad t = \frac{t'U_\infty}{R}, \tag{6}$$

where a prime denotes a dimensional value.

The unsteady diffusion equation is used by considering that the physical time for reaching the steady-state concentration may be longer than that for reaching the steady state of the flow field.

The boundary conditions are expressed as follows:

(1) at the uniform free-stream condition $(r\to\infty)$,

$$\frac{\psi_2}{r^2}\to\tfrac{1}{2}\sin^2\vartheta, \tag{7}$$

$$C\to 0; \tag{8}$$

(2) on the axis of symmetry $(\vartheta = 0, \pi)$,

$$\psi_i = \omega_i = \frac{\partial C}{\partial\vartheta} = 0; \tag{9}$$

(3) at the outer interface of the encapsulated drop ($r = \zeta$),

$$\frac{\partial \psi_1}{\partial \vartheta} = \frac{\partial \psi_2}{\partial \vartheta} = 0 \qquad \text{(no flow across the interface)}, \qquad [10]$$

$$\frac{\partial \psi_1}{\partial r} = \frac{\partial \psi_2}{\partial r} \qquad \text{(continuity of tangential velocity)}, \qquad [11]$$

$$\frac{\partial}{\partial r}\left(\frac{1}{r^2}\cdot\frac{\partial \psi_2}{\partial r}\right) = \kappa \frac{\partial}{\partial r}\left(\frac{1}{r^2}\cdot\frac{\partial \psi_1}{\partial r}\right) \qquad \text{(continuity of tangential stress)} \qquad [12]$$

and

$$C = 1 \qquad \text{(uniform constant concentration)}; \qquad [13]$$

(4) at the inner interface of the encapsulated drop ($r = 1$),

$$\frac{\partial \psi_1}{\partial \vartheta} = 0 \qquad \text{(no flow across the interface)}, \qquad [14]$$

$$\frac{\partial}{\partial r}\left(\frac{1}{r^2}\cdot\frac{\partial \psi_1}{\partial r}\right) = 0 \qquad \text{(zero tangential stress)}, \qquad [15]$$

where $\kappa = \eta_1/\eta_2$ is the viscosity ratio.

The initial condition is as follows:

$$C = \begin{cases} 0 & \text{at } r > \zeta \\ 1 & \text{at } r = \zeta. \end{cases} \qquad [16]$$

In this paper, Re, ζ (radius ratio), κ, γ (density ratio $= \rho_1/\rho_2$), Sc and K are fundamental dimensionless parameters.

Numerical Method of Solution

An exponential step size in the radial direction was used by employing the substitution $r = \exp(Z)$ and taking equal intervals in Z. After this transformation, [1] and [2] were rewritten as finite difference equations using the centered spatial differences of second-order accuracy and were solved by the SOR (successive over relaxation) method. Equation [5] was also rewritten using the centered spatial differences of second-order accuracy and the backward time differences of second-order accuracy. Equation [5] was solved by the ADI (alternate direction iterative) method. This numerical code for C was developed based on the multipoint implicit method. In the calculation mesh system, the radial step size for Z was 0.0125, the angular step size was 1.5° and the dimensionless position of the outer boundary was 54.6, which corresponded to $r = \infty$. The SOR and ADI procedures were repeated until ψ, ω and C changed by less than a specified tolerance per iteration. The tolerance was chosen to be 0.0001 for ψ and ω, and 0.00001 for C. The time step for C was 0.01.

RESULTS AND DISCUSSION

Figure 2 shows a sample of time-dependent concentration contours, $C = 0.1n$ ($n = 1$ to 10). The values of κ and γ are decided by considering that black ink is the medium in phase 1 and kerosene is the medium in phase 2 (e.g. Hashimoto & Kawano 1990). Figure 2 shows that the high concentration region (often referred to as a concentration wake) is convected downstream from the point close to the flow separation. Figure 2(d) shows that a pseudo-steady state seems to be achieved. This state means that the mean Sherwood number Sh_m defined in [18] reaches the unchanging constant [tolerance is 0.0001 per time step and gives the value $t = 14.96$ shown in figure 2(d)]. In this paper, the local Sherwood number Sh and Sh_m are defined as follows:

$$Sh = \frac{2\zeta' N}{D(C_1 - C_\infty)} = -2\left(\frac{\partial C}{\partial Z}\right)_{Z = Z_1} \qquad [17]$$

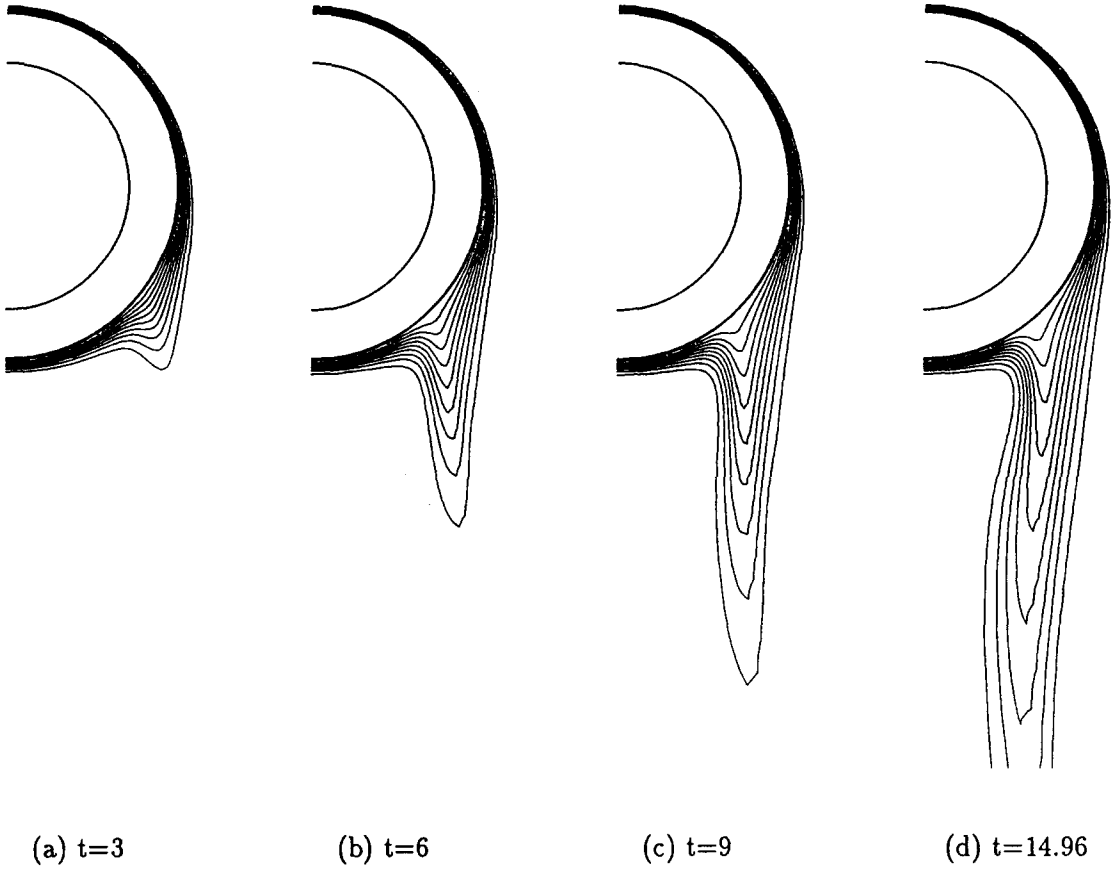

Figure 2. Time-dependent concentration contours at Re = 200, Sc = 10, $\zeta = 1.4$, $\kappa = 0.959$, $\gamma = 1.21$ and $K = 0$.

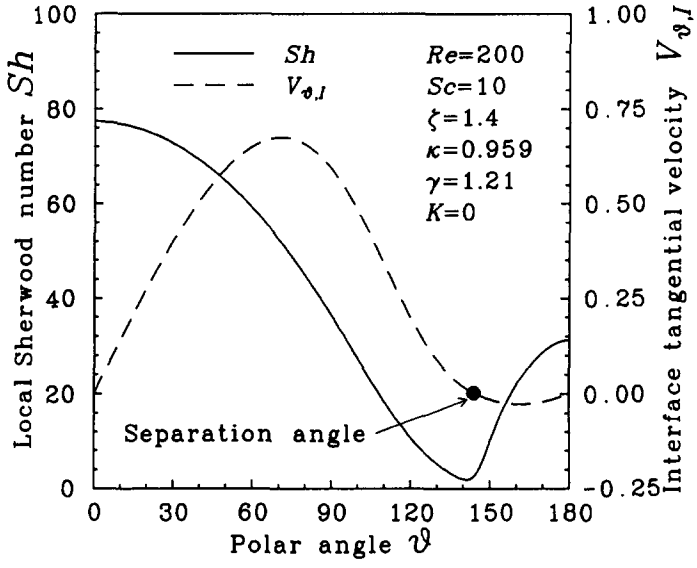

Figure 3. Relationships of Sh and $V_{\vartheta,I}$ to ϑ.

and

$$\mathrm{Sh}_m = -\int_0^{\pi} \left(\frac{\partial C}{\partial Z}\right)_{Z=Z_1} \sin\vartheta \cdot \mathrm{d}\vartheta, \qquad [18]$$

where N is the local mass diffusion flux expressed by Fick's law at $r = \zeta$ and Z_1 satisfies $\zeta = \exp(Z_1)$. We will discuss the pseudo-steady state in the following. Figure 3 shows the relationship of Sh to the polar angle ϑ at the values of Re, Sc, ζ, κ, γ and K shown in figure 2. The relationship of the interface tangential velocity $V_{\vartheta,1}$ to ϑ and the flow separation point determined from the $V_{\vartheta,1}$-curve are also shown in figure 3. At Re = 200, Sh decreases monotonously from the front stagnation point to the flow separation point. The increased Sh at the rear of the encapsulated drop is caused by the action of the recirculating attached wake shown in figure 1. The minimum Sc occurs near the flow separation point. If the angular diffusion is negligible, the minimum occurs exactly at the flow separation point. Figure 4 shows the effect of Sc on the concentration contours. The downstream concentration contours are distorted by the recirculatory flow in the wake shown in figure 1. The ratio of distortion increases as Sc increases. At constant Re, increasing Sc narrows the concentration wake and thins the concentration boundary layer [see figure 5(c)]. Comparisons between concentration contours (right half) and the streamlines (left half) for various Re are shown in figure 5. The values of ψ are equal to -5×10^{-2}, -2×10^{-2}, -1×10^{-2}, -5×10^{-3}, -2×10^{-3}, -1×10^{-3}, 0, 2×10^{-4}, 5×10^{-2}, 0.2, 0.5, 1 and 2. Even at Re = 1, the asymmetry vs upstream and downstream appears in the concentration contours. At Re = 50, where a flow separation initially appears at approx. $\vartheta = 172°$, the concentration wake locates behind the encapsulated drop. At Re = 100, where a flow separation occurs at $\vartheta = 150°$ and a large recirculating attached wake exists, the downstream concentration wake is narrowed and the concentration contours are

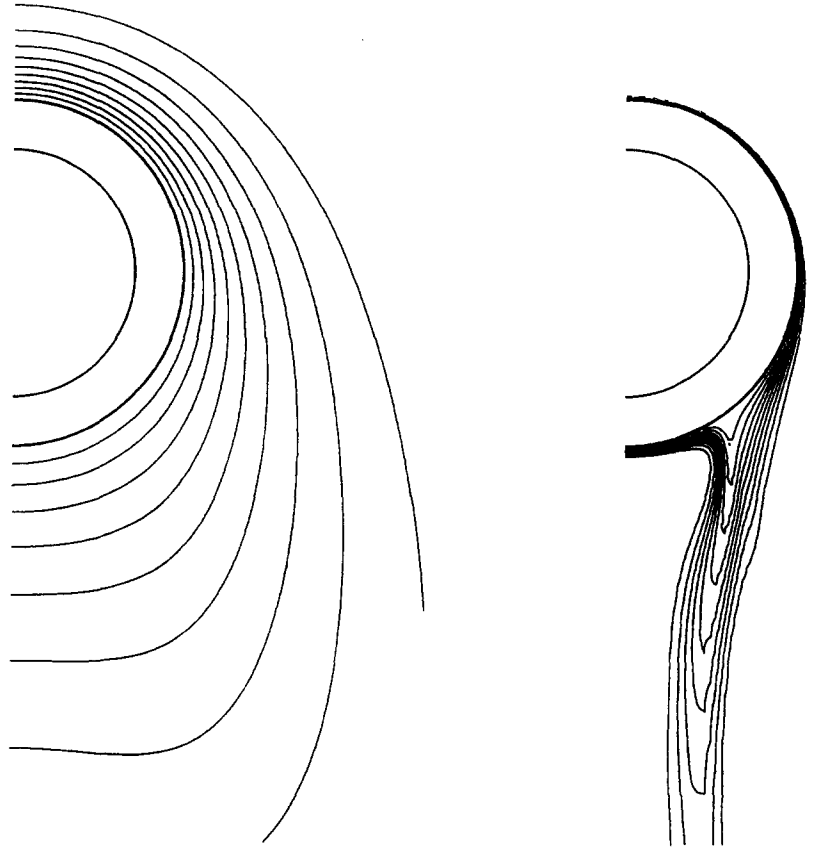

(a) $Sc = 0.1$ (b) $Sc = 100$

Figure 4. Concentration contours for various Sc at Re = 100, $\zeta = 1.4$, $\kappa = 0.959$, $\gamma = 1.21$ and $K = 0$.

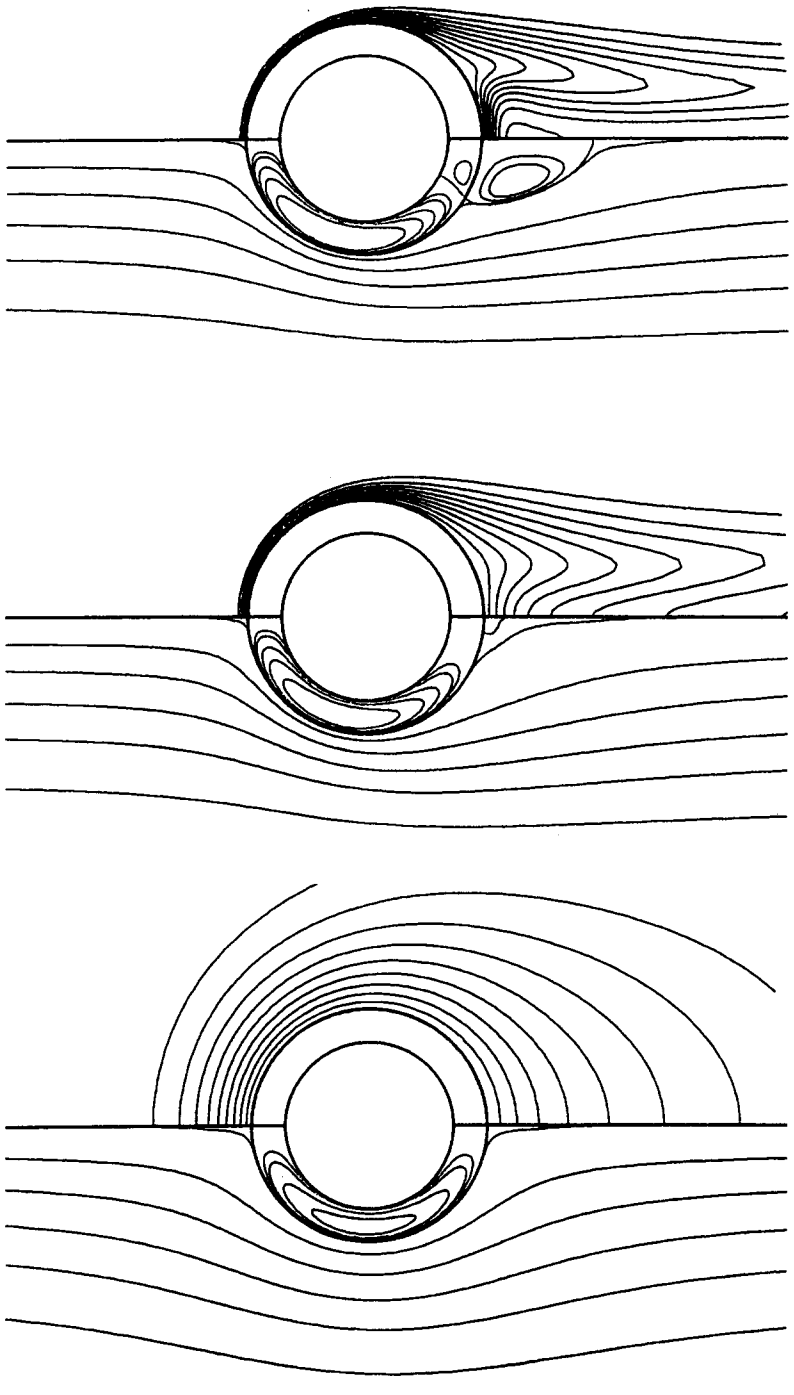

Figure 5. Comparisons between concentration contours (right-hand side) and streamlines (left-hand side) for various Re at Sc = 10, $\zeta = 1.4$, $\kappa = 0.959$, $\gamma = 1.21$ and $K = 0$.

distorted by the recirculatory flow in the wake. Increasing Re at constant Sc also narrows the concentration wake and thins the concentration boundary layer [see figure 2(d)]. These results have the same qualitative tendency as the results for a rigid sphere. Figure 6 shows the relationship of Sh_m to Re for various Sc. When $Pe \to 0$, the numerical values approach the analytical value ($Sh_m = 2$), where $Pe = Re \cdot Sc$ is the Péclet number. Sh_m increases as Re and Sc increase. In figure 6, the present numerical values are compared with those given by previous well-known equations as follows (e.g. Clift *et al.* 1978):

empirical correlations for a rigid sphere,

$$Sh_m = 2 + 0.6 \cdot Re^{1/2}Sc^{1/3}; \quad [19]$$

analytical equation in a Stokes flow field for a rigid sphere at $Re \to 0$,

$$Sh_m = 1 + (1 + Pe)^{1/3}; \quad [20]$$

analytical equation in a Hadamard–Rybczynski flow field for a gas bubble at $Re \to 0$ *and in* $Pe > 100$,

$$Sh_m = \frac{2}{\sqrt{3\pi}} Pe^{1/2}; \quad [21]$$

and

analytical equation in a potential flow field in $Pe \gg 1$,

$$Sh_m = \frac{2}{\sqrt{\pi}} Pe^{1/2}. \quad [22]$$

Comparing all the numerical values with those in [19], it is found that Sh_m is larger than that for a rigid sphere (e.g. at $Sc = 10$ in figure 6). This is caused by the mobility of the encapsulated drop outer interface shown in figure 3. The numerical values are between the values for a rigid sphere

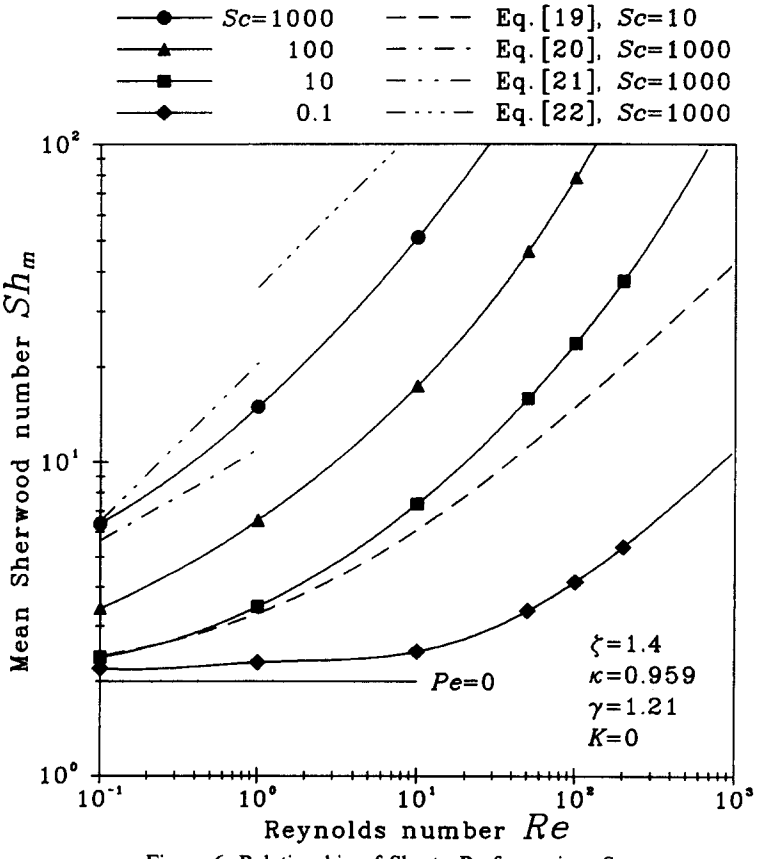

Figure 6. Relationship of Sh_m to Re for various Sc.

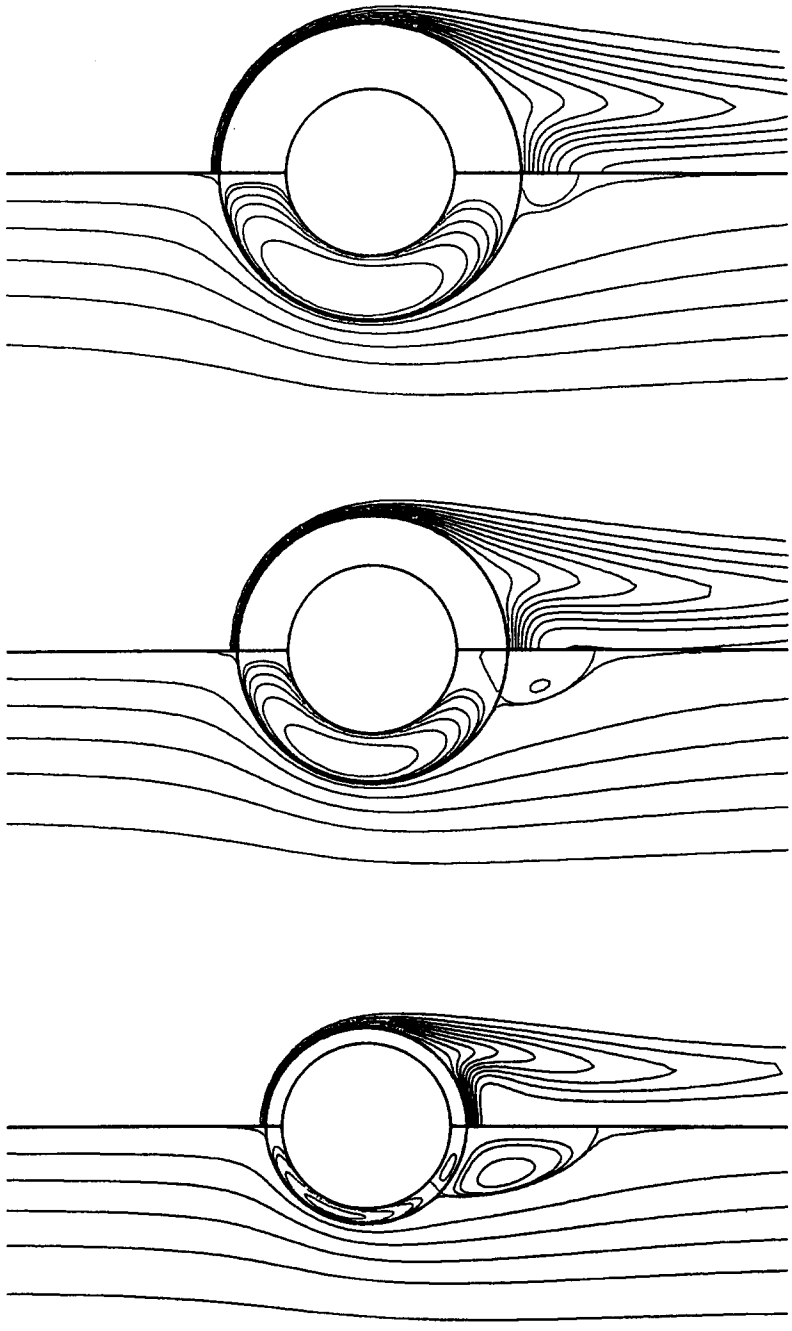

Figure 7. Comparisons between concentration contours (right-hand side) and streamlines (left-hand side) for various ζ at $\mathrm{Re} = 100$, $\mathrm{Sc} = 10$, $\kappa = 0.959$, $\gamma = 1.21$ and $K = 0$.

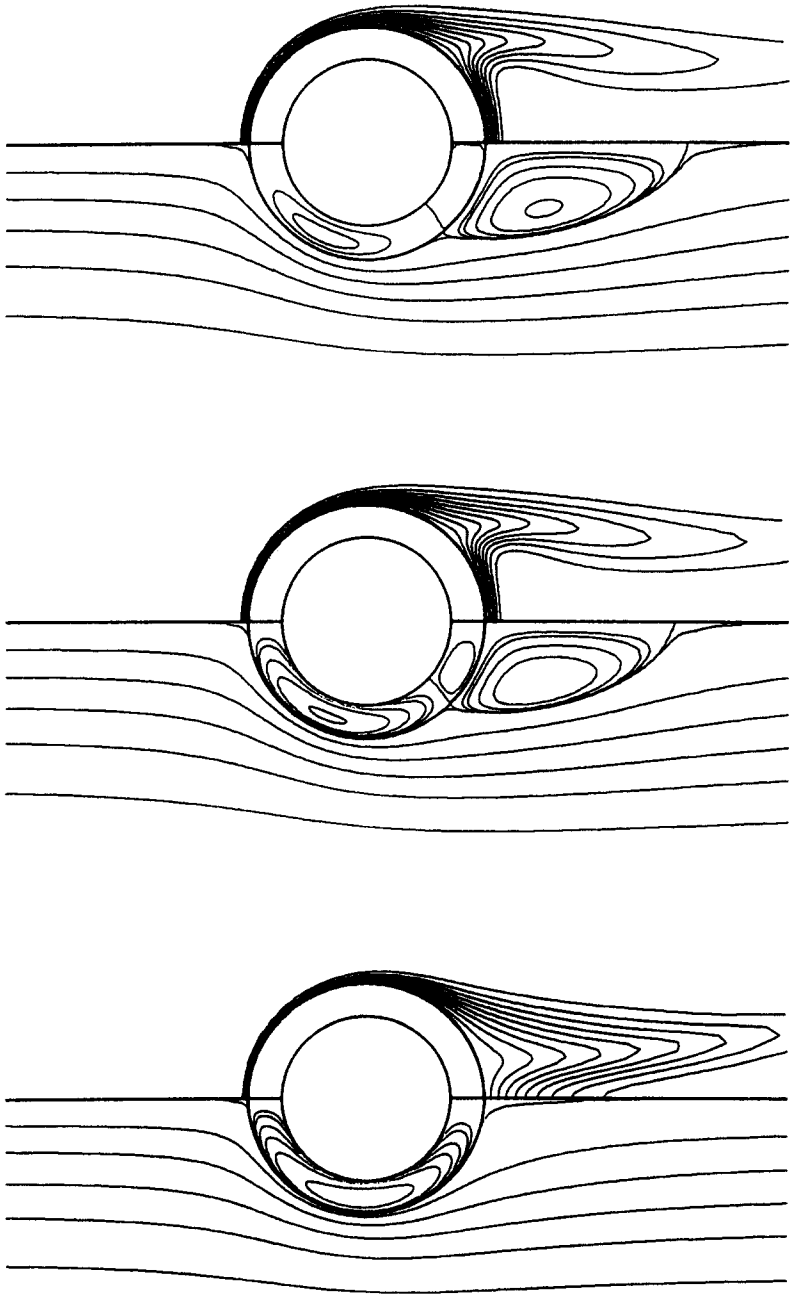

Figure 8. Comparisons between concentration contours (right-hand side) and streamlines (left-hand side) for various κ at $\mathrm{Re} = 100$, $\mathrm{Sc} = 10$, $\zeta = 1.4$, $\gamma = 1.21$ and $K = 0$.

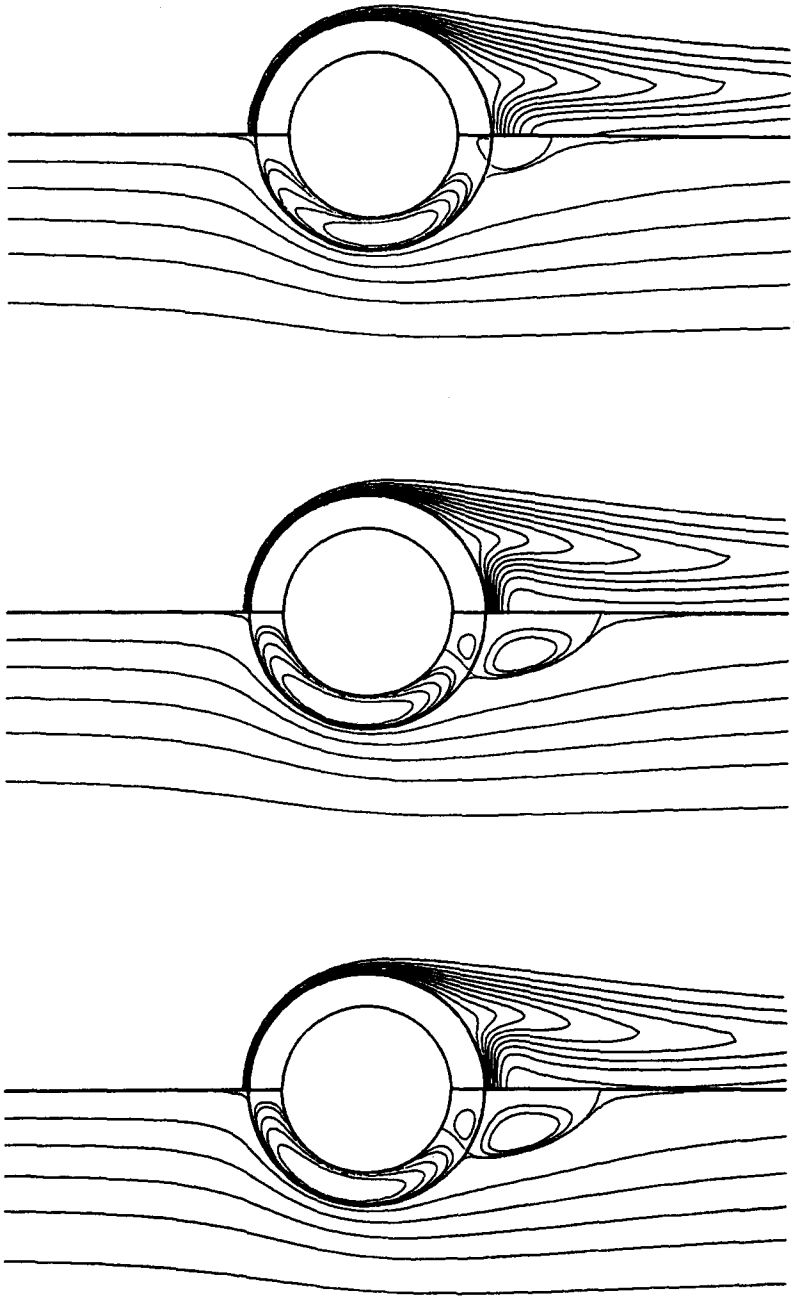

Figure 9. Comparisons between concentration contours (right-hand side) and streamlines (left-hand side) for various γ at Re = 100, Sc = 10, $\zeta = 1.4$, $\kappa = 0.959$ and $K = 0$.

obtained from [20] and for a gas bubble obtained from [21] at Sc = 1000 and at low Re in figure 6. These ranges of Re and Sc are significant when the encapsulated drop is applied as an artificial red corpuscle (in the blood flow, the ranges are approx. Re < 8.0 and Sc > 1181 at 30°C). Furthermore, numerical values at Sc = 1000 and at high Re seem to approach the values obtained from [22]. For a much higher Pe range than all the data shown in figure 6, the extremely fine calculation mesh system is needed for capturing an extremely thin concentration boundary layer.

Comparisons between the concentration contours (right half) and the streamlines (left half) for various ζ, κ and γ are shown in figures 7, 8 and 9, respectively. The flow pattern around an encapsulated drop approaches that around a rigid sphere at $\zeta \to 1$ (Rushton & Davies 1983) and at $\kappa \to \infty$, that around a liquid drop at $\zeta \to \infty$ and that around a gas bubble at $\kappa \to 0$. In figure 7, it should be noted that the values of ψ are made dimensionless using the characteristic length R for the reasons of the above numerical method; although Re is made dimensionless using the characteristic length ζ'. Decreasing ζ and increasing κ narrow the concentration wake, because they decrease the mobility of an outer interface and develop an attached wake behind the encapsulated drop. In figures 7(a), 8(b) and 8(c), the concentration contours are distorted and the area where $C = 0$ is formed at the rear of the encapsulated drop by the strong recirculatory flow in the wake. Figures 7(c), 9(b) and 9(c) are only for reference because the encapsulated drop cannot move upward for the ζ and γ cases in actual phenomena. Comparing figure 9 with figures 7 and 8, it is found that the effect of γ on the concentration contours is weaker than the effects of ζ and κ. Increasing γ means increasing the inertia effect on the spherical phase 1 motion and narrowing the attached wake. It was reported that the effect of increasing γ on the mobility of the outer interface was very small (Kawano & Hashimoto 1992). Then, not only the effect of the mobility of the outer interface but also the effect of the flow separation characteristics on the concentration contours is significant. Figure 10 shows the relationships of Sh_m to ζ, κ and γ. From figure 10, it is found that Sh_m, which is related closely to the concentration boundary layer thickness, increases as ζ increases and as κ decreases. Note also that $V_{3,1}$ increases as ζ increases and as κ decreases. Sh_m increases as the mobility becomes large. It is found that the dependence of Sh_m on γ is not so strong but the inertia effect of phase 1 seems to appear in $\gamma \geqslant 10$. Furthermore, at $\zeta \to 1$ or at $\kappa \to \infty$, numerical values seem to approach Sh_m for a rigid sphere ($Sh_m = 14.9$) obtained from [19].

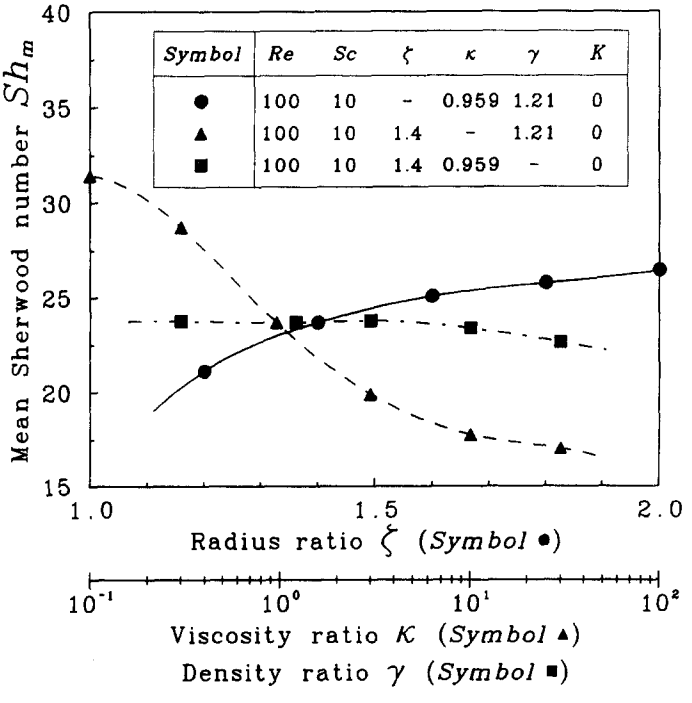

Figure 10. Relationships of Sh_m to ζ, κ and γ.

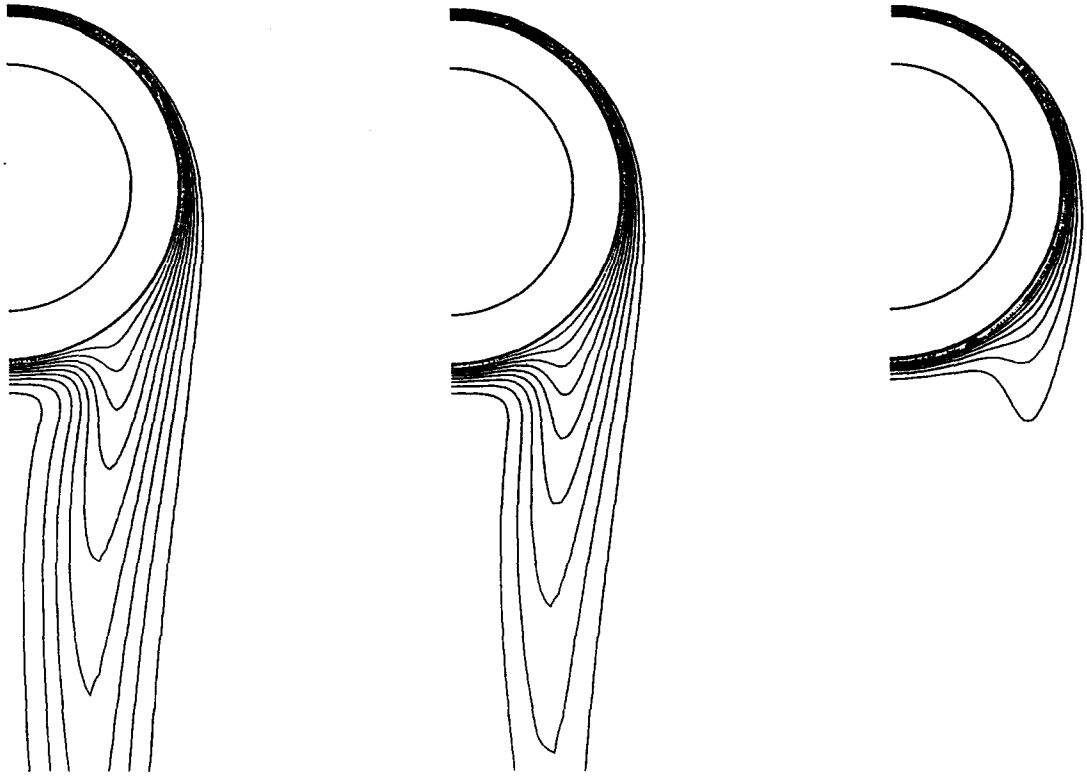

(a) $K = 1$ (b) $K = 10$ (c) $K = 100$

Figure 11. Concentration contours for various K at Re = 100, Sc = 10, $\zeta = 1.4$, $\kappa = 0.959$ and $\gamma = 1.21$.

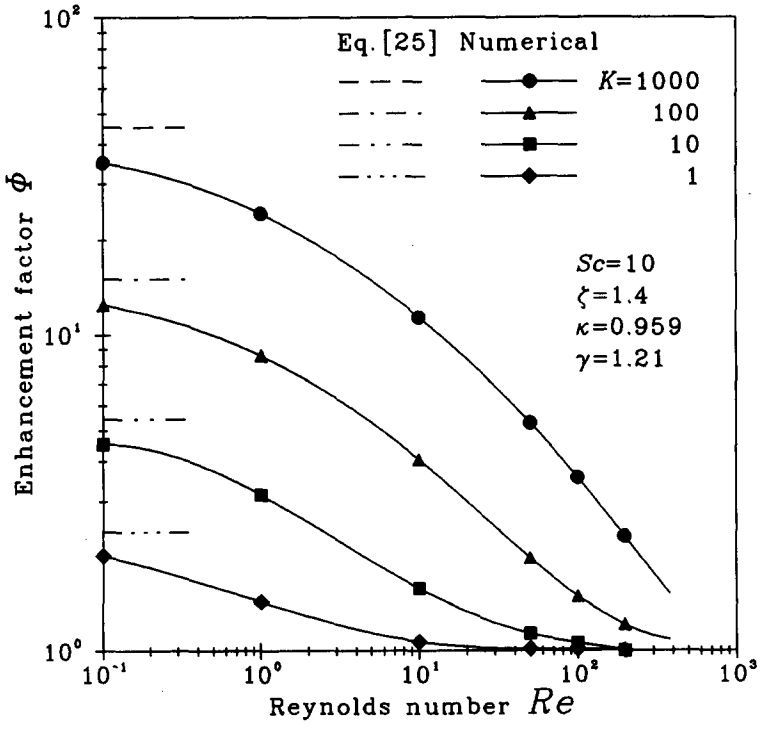

Figure 12. Relationship of Φ to Re for various K.

On the other hand, Sh_m for a gas bubble or for a liquid drop can be predicted roughly by the following equation for $Re > 70$ and $\kappa < 2$ (e.g. Clift *et al.* 1978):

$$Sh_m = \frac{2}{\sqrt{\pi}}\left[1 - \frac{1}{Re^{1/2}}(2.89 + 2.15\kappa^{0.64})\right]^{1/2} Pe^{1/2}. \quad [23]$$

The present numerical values seem to approximately approach Sh_m for a gas bubble ($Sh_m = 35.7$ obtained from [22] or $Sh_m = 30.1$ obtained from [23]) at $\kappa \to 0$ and for a liquid drop ($Sh_m = 25.3$ obtained from [23]) at $\zeta \to \infty$. In practical use, the results of figures 7, 8 and 10 suggest that the mass transfer characteristics can be controlled easily by selecting ζ and κ.

Figure 11 shows the concentration contours for various K. The concentration wake becomes narrow as K increases because the chemical reaction becomes active in the high concentration region. A lot of diffusing species (material A) would disappear at large K in the concentration wake. Figure 12 shows the relationship of enhancement factor Φ to Re for various K. The enhancement factor is defined as $\Phi = Sh_{m,C}/Sh_m$, whereby the subscript C indicates the value with the chemical reaction. It is found that Φ increases as K increases and as Re decreases. Assuming that $V = 0$ in a steady state, the analytical solution of [5] is obtained as follows:

$$C = \frac{\zeta}{r}\exp(\zeta\sqrt{K} - r\sqrt{K}). \quad [24]$$

Then, from [24], Φ is expressed as follows:

$$\Phi = 1 + \zeta\sqrt{K}. \quad [25]$$

Figure 12 shows that the numerical values approach analytical values obtained from [25] at small Re. The Φ approaches 1 at large Re because the concentration wake, where the chemical reaction is active, becomes narrow as Re increases, as shown in figure 5. Furthermore, the effect of the chemical reaction term is small ($1 \leqslant \Phi \leqslant 1.14$) for $K \leqslant 10$ and $Re \geqslant 50$ at the values of Sc, ζ, κ and γ indicated in figure 12.

Finally, we will discuss the time for reaching a pseudo-steady state t_S. In an encapsulated drop, there is a large circulation in phase 1 at small Re, as shown in figure 5(a), and there are two circulations in phase 1 and a circulation wake behind the drop at relatively large Re, as shown in figure 5(c). Then, t_S at high Pe must be significantly longer than any circulation duration. However, the circulation duration depends strongly on Re, ζ and the physical properties of the liquids. For instance, the circulation duration along $\psi_2 = -2 \times 10^{-3}$ of the wake was estimated roughly to be 13 at $Re = 200$, $\zeta = 1.4$, $\kappa = 0.959$ and $\gamma = 1.21$ and the circulation duration in phase 1 increases infinitely at $\zeta \to 1$ or at $\kappa \to \infty$. However, the present representative numerical data of Sh_m were checked for the longer time ($t = 50$ and 100), as shown in table 1. The maximum deviation rate between Sh_m for the pseudo-steady state and the Sh_m at $t = 100$ is 6.8% i.e. the values of Sh_m seem to be almost unchanged. This suggests that the definition of the pseudo-steady state in the present paper has a meaning in the practical engineering field.

CONCLUSION

To investigate the mass transfer phenomenon around a moving encapsulated drop, the Navier–Stokes equations and the diffusion equation including the first-order chemical reaction term

Table 1. Representative numerical data for Sh_m and t_S

Re	Sc	ζ	κ	γ	K	t_S	Sh_m	$Sh_{m,t=50}$	$Sh_{m,t=100}$
0.1	0.1	1.4	0.959	1.21	0	0.48	2.20	2.07	2.05
200	10	1.4	0.959	1.21	0	14.96	37.3	36.9	36.4
10	1000	1.4	0.959	1.21	0	20.24	51.0	51.0	51.0
100	10	1.2	0.959	1.21	0	17.79	21.1	20.7	20.4
100	10	2.0	0.959	1.21	0	19.34	26.4	26.4	26.4
100	10	1.4	0.1	1.21	0	6.29	31.4	31.4	31.4
100	10	1.4	30	1.21	0	19.19	17.0	16.7	16.3
100	10	1.4	0.959	0.3	0	23.15	23.8	23.5	23.3
100	10	1.4	0.959	30	0	19.25	22.6	22.5	22.5
0.1	10	1.4	0.959	1.21	1000	0.08	83.6	83.6	83.6
200	10	1.4	0.959	1.21	1000	3.28	86.5	86.5	86.5

were solved by the multipoint implicit method under the condition of uniform interface concentration. Consequently, the mass transfer characteristics around a spherically concentric encapsulated drop moving at finite Re (up to 200) were investigated for the wide velocity range and for different fluid physical properties. Although the applications of the present study may be limited to a spherically concentric encapsulated drop with no surfactant (no interfacial tension gradients), the effect of finite-Re flow was discussed quantitatively. The main features of this study are as follows:

(1) The Sh_m for an encapsulated drop is larger than that for a rigid sphere and depends on ζ and κ. The result suggests the possibility of developing a highly functional mass exchanger by applying encapsulated drops as spherical liquid surfactant membranes with selectivity.
(2) The Sh_m increases as ζ increases and as κ decreases because of the mobility of the encapsulated drop outer interface. The dependence of Sh_m on γ is very weak. The effects of Re, Sc and K on the mass transfer characteristics for the encapsulated drop may have the same qualitative tendency as those for a gas bubble, for a liquid drop and for a rigid sphere.
(3) There is a strong dependence of the mass transfer characteristics of the encapsulated drop on the outer interface mobility and on the flow separation characteristics around the encapsulated drop.

REFERENCES

CLIFT, R., GRACE, J. R. & WEBER, M. E. 1978 *Bubbles, Drops, and Particles*, pp. 49–50, 135–136, Academic Press, New York.

GREENE, G. A., CHEN, J. C. & CONLIN, M. T. 1988 Onset of entrainment between immiscible liquid layers due to rising gas bubbles. *Int. J. Heat Mass Transfer* **31,** 1309–1317.

HASHIMOTO, H. & KAWANO, S. 1989 Formation of encapsulated liquid drops in liquid–liquid–gas systems. In *Proc. Int. Conf. on Mechanics of Two-Phase Flows* (Edited by LEE, R. S. L. & DURST, F.), Taipei, Taiwan, pp. 341–346.

HASHIMOTO, H. & KAWANO, S. 1990 A study on encapsulated liquid drop formation in liquid–liquid–gas systems: fundamental mechanism of encapsulated drop formation. *JSME Int. J. Ser. II* **33,** 729–735.

HASHIMOTO, H. & KAWANO, S. 1991 Sequential production of solid shells in liquid–liquid–gas systems. *Trans. JSME* **57B,** 2180–2185. In Japanese.

JOHNSON, R. E. & SADHAL, S. S. 1985 Fluid mechanics of compound multiphase drops and bubbles. *A. Rev. Fluid Mech.* **17,** 289–320.

KAWANO, S. & HASHIMOTO, H. 1990 A study on encapsulated liquid drop formation in liquid–liquid–gas systems: 2nd Report, instability of interfaces in a gas–liquid compound jet. *Trans. JSME* **56B,** 1652–1658. In Japanese.

KAWANO, S. & HASHIMOTO, H. 1992 Drag coefficient of a spherical encapsulated liquid drop. *JSME Int. J. Ser. II* **35,** 151–157.

KENDALL, J. M. 1986 Experiments on annular liquid jet instability and on the formation of liquid shells. *Phys. Fluids* **29,** 2086–2094.

LANDMAN, K. A. 1985 Stability of a viscous compound fluid drop. *AIChE Jl* **31,** 567–573.

LEE, C. P. & WANG, T. G. 1986 A theoretical model for the annular jet instability. *Phys. Fluids* **29,** 2076–2085.

LEE, C. P. & WANG, T. G. 1988 The centering dynamics of a thin liquid shell ir capillary oscillations. *J. Fluid Mech.* **188,** 411–435.

LEE, M. C., KENDALL, J. M. JR, BAHRAMI, P. A. & WANG, T. G. 1986 Sensational spherical shells. *Aerosp. Am.* **24,** 72–76.

LI, N. N. 1971 Permeation through liquid surfactant membranes. *AIChE Jl* **17,** 459–463.

MORI, Y. H. 1987 Artificial transformation of the direct-contact condensation pattern of steam bubbles in a hydrophobic liquid medium. *Trans. ASME Jl Heat Transfer* **109,** 1007–1012.

OGUZ, H. N. & SADHAL, S. S. 1987 Growth and collapse of translating compound multiphase drops: analysis of fluid mechanics and heat transfer. *J. Fluid Mech.* **179,** 105–136.

RUSHTON, E. & DAVIES, G. A. 1983 Settling of encapsulated droplets at low Reynolds numbers. *Int. J. Multiphase Flow* **9,** 337–342.

SADHAL, S. S. & OGUZ, H. N. 1985 Stokes flow past compound multiphase drops: the case of completely engulfed drops/bubbles. *J. Fluid Mech.* **160,** 511–529.

STONE, H. A. & LEAL, L. G. 1990 Breakup of concentric double emulsion droplets in linear flows. *J. Fluid Mech.* **221,** 123–156.

TSAMOPOULOS, J. A. & BROWN, R. A. 1987 Dynamic centering of liquid shells. *Phys. Fluids* **30,** 27–35.

VUONG, S. T. & SADHAL, S. S. 1989a Growth and translation of a liquid–vapour compound drop in a second liquid. Part 1. Fluid mechanics. *J. Fluid Mech.* **209,** 617–637.

VUONG, S. T. & SADHAL, S. S. 1989b Growth and translation of a liquid–vapour compound drop in a second liquid. Part 2. Heat transfer. *J. Fluid Mech.* **209,** 639–660.